Modeling optical constants from the absorption of organic thin films using a modified Lorentz oscillator model

Dutta, Arpan

2022-07-01

Dutta , A , Tiainen , V , Qureshi , H A , Duarte , L & Toppari , J J 2022 , ' Modeling optical constants from the absorption of organic thin films using a modified Lorentz oscillator model ' , Optical materials express , vol. 12 , no. 7 , pp. 2855-2869 . https://doi.org/10.1364/OME.459938

http://hdl.handle.net/10138/346704
https://doi.org/10.1364/OME.459938

Research Article Vol. 12, No. 7 / 1 Jul 2022 / Optical Materials Express 2855
Optical Materials EXPRESS

Modeling optical constants from the absorption of organic thin films using a modified Lorentz oscillator model

ARPAN DUTTA,[1,4] VILLE TIAINEN,[1] HASSAN ALI QURESHI,[1,2] LUÍS DUARTE,[1,3] AND J. JUSSI TOPPARI[1,5]

[1]*Nanoscience Center and Department of Physics, University of Jyväskylä, P.O. Box 35, FI-40014, Finland*
[2]*Currently with Department of Mechanical and Materials Engineering, University of Turku, FI-20014, Finland*
[3]*Currently with Department of Chemistry, University of Helsinki, P.O. Box 55, FI-00014, Finland*
[4]*arpan.a.dutta@jyu.fi*
[5]*j.jussi.toppari@jyu.fi*

Abstract: Optical constants of organic thin films can be evaluated using the Lorentz oscillator model (LOM) which fails to fit inhomogeneously broadened absorption of highly concentrated molecular films. In modified LOM (MLOM), the inhomogeneous broadening is implemented through a frequency-dependent adjustable broadening function. In this work, we evaluate the optical constants of rhodamine 6G doped poly-vinyl alcohol thin films with varying doping concentration (including also extensively high concentrations) using MLOM, which outperforms LOM by showing a better agreement with the experimental results. Our proposed method provides a way to accurately determine optical constants of isotropic organic thin films only from their absorption spectra without spectroscopic ellipsometry.

1. Introduction

Organic thin films are popular in photovoltaics [1–3] and optoelectronics [4–6] due to their compatibility with cost-effective synthesis procedures and large-scale manufacturing techniques on flexible substrates [1,2]. Such thin films usually consist of a polymer matrix doped with photoactive organic molecules (e.g. dyes) acting as Frenkel excitons [7]. These dye-doped thin films have potential applications in resonant nanophotonics [8–10] and their excitonic properties [7,11] can be used for enhancing light-matter coupling within the optical devices [12,13] even to a limit of strong coupling [10,14–17].

Optimal design of novel excitonic devices based on dye-doped organic thin films requires precise modeling of the local excitonic absorption bands manifested in those thin films [5–13]. Such modeling, however, often becomes challenging due to a lack of accurate information on the optical constants of the thin solid films, i.e., their wavelength-dependent complex refractive index and complex dielectric function. Usually these optical constants can be evaluated over the spectral region of interest using a spectral fitting involving a suitable dispersion relation [18,19]. In such fitting method, the experimental reflection, transmission and absorption spectra of the films are fitted by the corresponding theoretically calculated ones using a least squares fitting procedure where the theoretical calculation uses the optical constants derived from the dispersion model [18]. Here, a pointwise optimization approach is employed, in which an objective function representing the degree of dissimilarity between the experimental and the theoretical spectra is minimized at all spectral points under reasonable physical constraints to attain proper accuracy in the optical constant values [18–21].

The choice of dispersion model plays a key role in the spectral fitting. The absorption of an organic solid, for example, the local excitonic absorption band of a dye-doped polymer

#459938 https://doi.org/10.1364/OME.459938
Journal © 2022 Received 31 Mar 2022; revised 17 Jun 2022; accepted 20 Jun 2022; published 29 Jun 2022

Optical Materials EXPRESS

film *ideally* should follow a Lorentzian profile [19] and hence, the corresponding dielectric function can be modelled via Lorentz oscillator model (LOM) [22,23]. The LOM provides lowest number of fitting parameters and inherent consistency with the Kramers-Kronig relation. The damping factor in LOM is a measure of the linewidth of the Lorentzian shaped absorption band and considered as a constant resulting from both the homogeneous broadening intrinsic to any molecular system [18,19,23], as well as lifetime broadening.

However, in the case of a highly concentrated molecular film, the system is an ensemble of numerous molecules doped in a polymeric medium. Increasing the doping concentration of such dye-doped polymer films usually results in significant changes in their absorption spectra [14,24]. This is because the system shifts away from the above-mentioned *ideal* case resulting in an inhomogeneously broadened absorption profile which does not follow a true Lorentzian or pure Gaussian shape [19,24–27]. Several factors are responsible for this inhomogeneous broadening such as formation of molecular aggregates, vibrational transitions accompanied with the electronic transitions, polycrystallinity of the doped film, and interaction of dye molecules with their polymeric surrounding having impurities/defects to name few [19,25–29]. The situation is too complicated to be fully determined from an experimental absorption spectrum since exact contributions from the different factors of inhomogeneity are unknown. Hence, LOM fails to extract the accurate dielectric function from an inhomogeneously broadened absorption [19,25–27].

This issue can be addressed by incorporating modifications in LOM such as – either using a higher number of oscillators [25] or using Gaussian/Voigt profiles to fit the absorption lineshape via convolution/superposition of (one or more) Lorentzian and Gaussian functions [24,27]. However, neither of these approaches are numerically optimal. Use of a higher number of oscillators involves a higher number of fitting parameters which makes the spectral fitting more complex and less meaningful for interpretation. On the other hand, Gaussian/Voigt functions may provide better fit to the absorption profile, but they lack analytically closed form and unlike LOM, there is no simple straightforward way to calculate the dielectric function from them [19,25].

Kim *et al.* [26] proposed a clever modification in LOM to overcome these shortcomings by including a spectrally dependent damping term working as an adjustable broadening function (ABF) [19,25,26]. The ABF includes two constant key parameters – the Lorentzian damping factor (γ) and an adjustable broadening parameter (α), and it is generalized for any arbitrary lineshape. This modified Lorentz oscillator model (MLOM) maintains an analytically closed form and hence, provides a simple straightforward way to calculate the dielectric function like LOM while it allows to fit any arbitrary broadening beyond the Lorentzian shape. For certain values of α, one can mimic the conventional spectral profiles, i.e., Lorentzian ($\alpha = 0$), Gaussian ($\alpha = 0.3$), and Voigt ($0<\alpha<0.3$) as well as most asymmetric/inhomogeneous lineshapes ($\alpha>0.3$) [19,25,26]. Since inhomogeneous broadening does not necessarily always result in Gaussian or Voigt profile but can take any arbitrary complex form [24,27–29], the incorporation of ABF in LOM is an efficient way to fit any arbitrary absorption lineshape and extract optical constants from it using minimal amount of fitting parameters. Consequently, MLOM provides better agreement with the experimental results compared to the conventional LOM [19,25].

Since the MLOM provides more realistic model, it can be used to calculate accurate absorption band which is then fitted with the measured one, by using the constants of the MLOM as the fitting parameters. This way MLOM enables accurate determination of optical constants of an organic thin film from its absorption band alone. By this method one can avoid the spectroscopic ellipsometry (SE) [30], which is usually needed for determination of the optical constants and often tricky to perform [18]. That is because SE is extremely sensitive to the quality of sample surface, type of substrate material, contamination [18,31], and because of this often requires assistance from other techniques such as surface plasmon spectroscopy to attain better accuracy [32].

Optical Materials EXPRESS

In this work, we propose a straightforward method to determine the optical constants of the isotropic organic thin films only from their absorption spectra. We evaluate the optical constants of rhodamine 6G (R6G) doped poly-vinyl alcohol (PVA) thin films with varying doping concentration (including also extensively high concentrations) from their experimental absorption using MLOM. The transfer-matrix method (TMM) [33–36] implemented in MATLAB [37] is used to calculate the theoretical absorption of the R6G films, which is further used to fit the experimental data using a least squares fitting method along with a pointwise optimization technique. Our proposed method outperforms the conventional LOM by yielding a better agreement with the experimental results, and avoids the need of ellipsometry. Our findings provide a way to model the local excitonic absorption bands of the isotropic organic thin films, using their evaluated optical constants, which is crucial for designing novel excitonic nanodevices.

2. Theory

The dispersive and complex dielectric function (ϵ) of a material can be described as

$$\epsilon(E) = \epsilon_1(E) + i\epsilon_2(E), \tag{1}$$

where E is the energy [19,25]. In LOM, the real (ϵ_1) and imaginary (ϵ_2) parts of the dielectric function are expressed as

$$\epsilon_1(E) = \epsilon_\infty + \sum_j \frac{f_j E_j^2 (E_j^2 - E^2)}{(E_j^2 - E^2)^2 + E^2\gamma_j^2}, \tag{2}$$

$$\epsilon_2(E) = \sum_j \frac{f_j E_j^2 E\gamma_j}{(E_j^2 - E^2)^2 + E^2\gamma_j^2}, \tag{3}$$

where $j = 0, 1, 2\ldots$ is the number of material resonances (transitions) with the resonant energy E_j, oscillator strength f_j, and damping rate γ_j [8,19,25], while ϵ_∞ represents the background dielectric constant within the exciton-energy region [14,38].

The corresponding real (n) and imaginary (k) parts of the refractive index (N) are

$$n(E) = \sqrt{\frac{\sqrt{\epsilon_1^2(E) + \epsilon_2^2(E)} + \epsilon_1(E)}{2}}, \tag{4}$$

$$k(E) = \sqrt{\frac{\sqrt{\epsilon_1^2(E) + \epsilon_2^2(E)} - \epsilon_1(E)}{2}}, \tag{5}$$

and

$$N(E) = n(E) + ik(E), \tag{6}$$

in their dispersive and complex form [19,25].

The LOM, i.e., Eq. (2) and Eq. (3), considers an ideal case where the damping rate (γ_j) is constant and consequently, the material resonances show homogeneous (Lorentzian) broadening where the resonance linewidth symmetrically broadens on both sides of the resonance peak energy (E_j) [22,23]. In the case of inhomogeneous broadening, the resonance lineshape for most of the time inherits Gaussian broadening or Voigt lineshape when combined with the homogeneous Lorentzian broadening [24,27]. Even higher inhomogeneous broadening usually results in asymmetric lineshapes with respect to the resonance peak (E_j) [19,24–29]. Therefore, the damping term has to be adjustable, i.e., frequency-dependent, to become adaptive for such

Optical Materials EXPRESS

arbitrary broadening [19,25,26]. To implement the inhomogeneity in the resonance linewidth Kim *et al.* [26] proposed an adjustable broadening function ($\gamma_j^{'}$) considered as

$$\gamma_j^{'}(E) = \gamma_j \exp\left[-\alpha_j \left(\frac{E - E_j}{\gamma_j}\right)^2\right], \tag{7}$$

where α_j is the adjustable broadening parameter associated with the material resonance j. Replacement of the damping rate γ_j in Eq. (2) and Eq. (3) by the frequency-dependent adjustable broadening function $\gamma_j^{'}$ will form the MLOM, which reduces to LOM for $\alpha_j = 0$ and can mimic any arbitrary lineshapes for $\alpha_j > 0$ [19,25,26].

In the spectral fitting, the fitting parameters (f_j, E_j, γ_j and α_j) are optimized by minimizing an objective function (Θ) defined as

$$\Theta = \sum_E \left[A_{exp}(E) - A_{TMM}(E)\right]^2, \tag{8}$$

where A_{exp} and A_{TMM} are the experimental and the TMM simulated absorption, respectively [20,21], calculated from the reflection (R) and the transmission (T) as $A = 1 - R - T$.

3. Materials and methods

3.1. Sample fabrication

Four R6G doped PVA films were fabricated with increasing R6G concentration on top of high optical quality BK7 glass substrates (Präzisions Glas and Optik GmbH, dimension: $15 \times 15\ mm^2$, thickness: 1 mm, surface roughness: ±0.10 mm). Also a bare PVA film without R6G doping was made as a reference sample. The substrates were cleaned by isopropanol and blown by nitrogen for drying. The R6G:PVA and bare PVA films were spin-coated on top of the clean substrates and hardened by baking for 3 min on a hot plate at 95 °C. The PVA crystals (Sigma-Aldrich, Hydrolyzed: 89%, CAS Number: 9002-89-5, Molecular Weight: 186) were dissolved in Millipore water at 90 °C to make a 10 wt% aqueous solution of PVA. The spin solutions were prepared by dissolving the required amount of solid R6G powder (ACROS Organics, Purity: 99%, CAS Number: 989-38-8, Molecular Weight: 479.017) in Millipore water and ethanol, and mixing that with 10 wt% aqueous solution of PVA to attain the target concentrations, i.e., 0.2 mol/L, 0.6 mol/L, 1.7 mol/L, and 5.2 mol/L. The KLA Tencor P-15 Profilometer was used for thickness characterization of the fabricated films and the recorded thicknesses were ~ 125 nm for all films. The profilometer data for one of our sample is reported in Appendix (Fig. 9).

3.2. Optical measurements

Steady-state reflection and transmission spectra of the fabricated films at a near-normal angle of incidence (10°) were measured in a custom-made optical setup where a white light source (Oriel 66182) was used for the excitation. The films were kept at the rotation axis of a goniometric stage facing the pseudo-collimated excitation light. The excitation was coming through a prism polarizer with the polarization axis perpendicular to the rotation plane. The excitation spot size on the sample surface was about 2 mm. The angle of incidence was adjusted manually by rotating the goniometric stage. The reflected and transmitted spectra of the films were collected using a fiber coupler assembly (ThorLabs F220SMA-A, f = 10.90 mm, NA = 0.25) connected to a fiber optic bundle (ThorLabs, model: BFL200HS02, 250 to 1200 nm, round to linear bundle, 7×200 µm core fibers, high-OH, SMA). The collected light was guided to a spectrometer consisting of a monochromator (Acton monochromator SP2150i, slit size: 100 µm, grating: 150 grooves/mm blazed at 500 nm) and CCD (Andor IVAC CCD DR-324B-FI, pixel size: $16 \times 16\ \mu m^2$), and the spectra were recorded in ASCII format.

Optical Materials EXPRESS

3.3. TMM simulation and spectral fitting

The experimental absorption (A_{exp}) of the R6G films was background corrected by subtracting the absorption of the reference sample (bare PVA film on BK7 glass) and in accordance with that, the R6G layers were considered in semi-infinite air in TMM simulation. The spectral fitting allowed an initial guess and two physical constraints, i.e., an upper and a lower bound for each fitting parameter. The initial guesses were fed to the MLOM to generate the initial values of n and k, which were used afterwards in TMM to calculate A_{TMM} and thereby, Θ. An optimization algorithm for finding the minimum of a constrained nonlinear multivariable function [39], as implemented in MATLAB, was employed to minimize Θ while the fitting parameters were allowed to vary between the upper and the lower bounds. The initial guesses and the physical constraints were estimated from a standard Voigt fit [40] on A_{exp} so that the fitting parameters can vary within a physically meaningful range.

4. Results and discussions

As explained earlier, the inhomogeneous broadening in the absorption of organic thin films can have various reasons and exact contributions from those different factors of inhomogeneity are impossible to know beforehand [19,25,27,29]. Therefore, application of an ABF via MLOM is a convenient way to fit such broadened and asymmetric spectra. The MLOM not only offers a quick and simple evaluation of optical constants from an experimental absorption spectrum but also provides a generalized model for all kinds of broadenings (Lorentzian, Gaussian, Voigt, and beyond) through the variation of an adjustable broadening parameter (α_j) [19,25,26].

To develop an insight on this adjustable broadening mechanism, we consider a single-oscillator MLOM framework representing material model for an organic thin film in a generic way. All the common parameters between LOM and MLOM are kept as constant, i.e., $f_0 = 0.03$, $\gamma_0 = 0.15$ eV, $E_0 = 2.3$ eV, and $\epsilon_\infty = 2.25$ while the adjustable broadening parameter (α_0) is varied, i.e., $\alpha_0 = 0, 0.15, 0.3, 3$. The optical constants are calculated using Eqs. (1–7) and subsequently used in TMM to simulate the corresponding absorption profiles. The simulated spectra are plotted in Fig. 1 along with the associated ABF in inset.

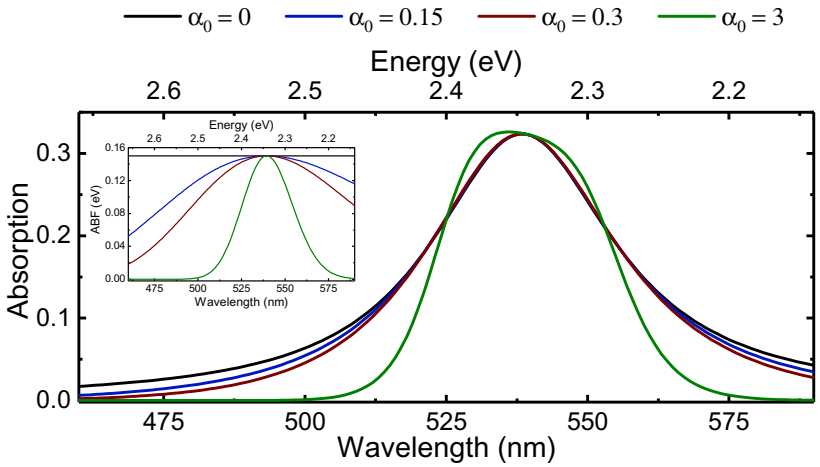

Fig. 1. MLOM/TMM simulated absorption spectra of a dye-doped polymer film for different values of adjustable broadening parameter (α_0). In the inset, spectral evolution of the corresponding adjustable broadening function is plotted. The other MLOM parameters are kept constant as $f_0 = 0.03$, $\gamma_0 = 0.15$ eV, $E_0 = 2.3$ eV, and $\epsilon_\infty = 2.25$.

Optical Materials EXPRESS

In the figure, $\alpha_0 = 0$ represents the true Lorentzian broadening while $\alpha_0 = 0.15$ and $\alpha_0 = 0.3$ show the shift from that *ideal* case towards Gaussian profiles via Voigt. It is evident that using only one oscillator with such small values of α_0 (i.e. Lorentzian/Gaussian/Voigt) is often not sufficient to fit absorption of organic films where electronic transitions are accompanied by many vibrational responses and usually multi-oscillator approaches or convolution of non-Lorentzian functions are needed [24,25,27]. However, for larger values of α_0, like $\alpha_0 = 3$, the absorption shows a flat and broad peak frequently observed in the absorption of highly concentrated molecular films as we will see in our experimental finding also. The associated changes in ABF (figure inset) clearly show the adaptive nature of the frequency-dependent damping since all the curves (except $\alpha_0 = 0$) show different degrees of spectral variation with varying α_0. Such adaptive broadening is essential to fit absorption of organic films possessing unintuitive sharp and subtle changes in their spectra. Therefore, the MLOM provides a much quicker, simpler and straightforward pathway to fit absorption of organic films with any arbitrary lineshape compared to the numerically cumbersome conventional methods (multi-oscillator/convolution of non-Lorentzians).

Before presenting our findings it is important to discuss our MLOM/TMM fitting procedure depicted as a flowchart in Fig. 2. The spectral fitting starts with assigning four fitting parameters (f_j, E_j, γ_j and α_j) as initial guesses. The initial guesses are fed to the MLOM to generate the initial values of n and k, which are then used in TMM to calculate A_{TMM}. An objective function (Θ) is employed along with the experimental absorption (A_{exp}) to quantify the accuracy of the fit and hence, the goal is to minimize Θ. An optimization algorithm [39] is employed for that purpose and during the optimization, the values of each fitting parameter is allowed to vary only between its corresponding physical constraints, i.e., an upper and a lower bound. The initial guesses and the physical constraints are estimated from a standard Voigt fit [40] on A_{exp} so that the fitting parameters can vary within a feasible range compatible with the experimental reality. The exit condition of the optimization is met when the minimal value for Θ is achieved, which in practice means that the change of the value between the consecutive iterations is smaller than the predefined error tolerance. The associated optimal parameters, i.e., optimal values of f_j, E_j, γ_j and α_j are then used to calculate the optical constants using Eqs. (1–7).

It should be noted here that our choice for a Voigt fit to estimate the initial guesses and the physical constraints is merely our chosen approach and our MLOM fitting method is not limited to any specific method for evaluation of those initial starting values. However, proper choice of constraints, i.e., the upper and the lower bounds is very important for multiple reasons. First of all, without suitable constraints, the optimization algorithm can converge into a physically meaningless solution with unrealistic fitting parameter values. Moreover, poor choice of constraints can make MLOM even invalid since for very large values of α_j, MLOM shows limitations by being inconsistent with the Kramers-Kronig relation and by producing splitting of single peaks which are unrealistic in nature [25].

Next we apply the method to a real experimental data as an example. The absorption spectra of the R6G films covering the spectral range of the local excitonic band of interest (i.e. 460 nm - 590 nm) are depicted in Fig. 3. In the figure, the experimental spectra (A_{exp}) are very slightly smoothed just to remove the excess noise and clarify the figure. The simulated absorption profiles are computed by TMM using the optical constants calculated from LOM ($A_{TMM(LOM)}$) and MLOM ($A_{TMM(MLOM)}$) with identical initial guesses and physical constraints (except those absent in LOM) for each concentration.

Two Lorentz oscillators are employed in LOM and MLOM to implement the R6G absorption having a molecular resonance (~ 540 nm, $j = 1$) and a vibronic shoulder (~ 503 nm, $j = 2$) at the blue side [24,41]. The amplitudes, the full widths at half maxima (FWHM) and the peak positions of the absorption bands present in the Voigt fit are used as initial guesses for f_j, γ_j and E_j, respectively. The initial guesses for α_j are estimated from the ratio between the Gaussian widths and the Lorentzian widths used in the Voigt fit while the non-resonant background within

Optical Materials EXPRESS

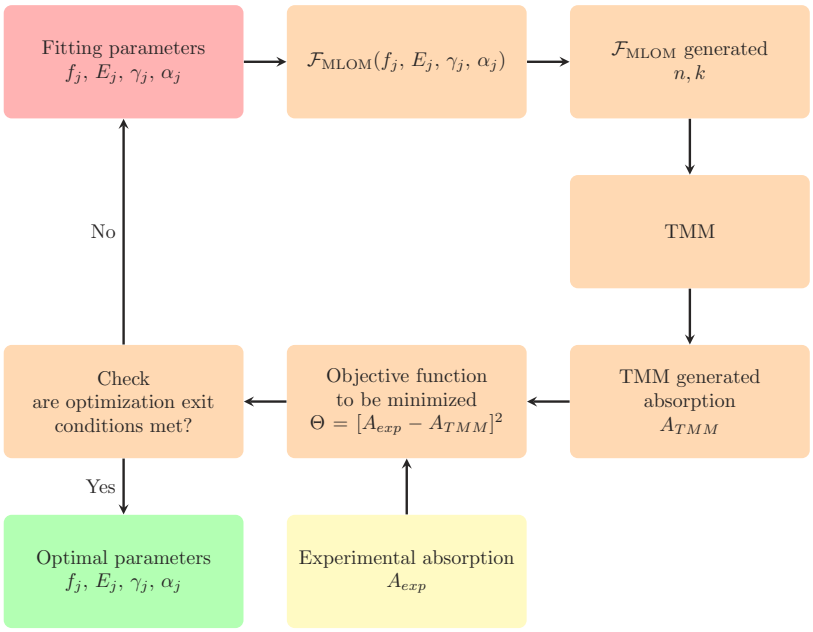

Fig. 2. Flowchart of the MLOM/TMM spectral fitting procedure.

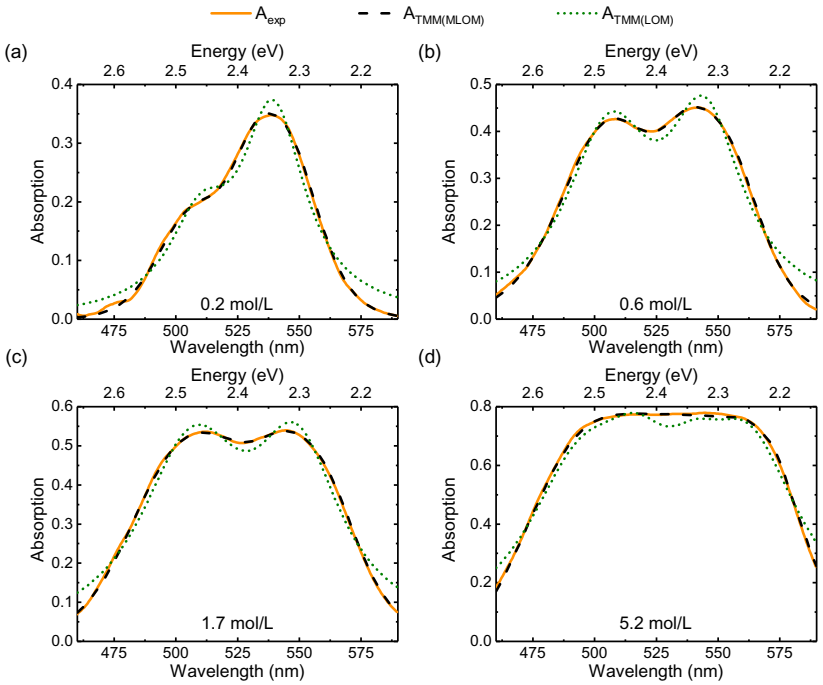

Fig. 3. Absorption profiles of the R6G films in the spectral range of the local excitonic band of interest for target concentrations: (a) 0.2 mol/L, (b) 0.6 mol/L, (c) 1.7 mol/L and (d) 5.2 mol/L. In the figure, $A_{TMM(LOM)}$ and $A_{TMM(MLOM)}$ represent the absorption profiles computed by TMM using the optical constants calculated from LOM and MLOM, respectively, while A_{exp} depicts the experimental (smoothed) absorption spectra.

Optical Materials EXPRESS

the exciton-energy region is considered as the dielectric constant of PVA, i.e., $\epsilon_\infty = 2.25$ [38,42]. The initial guesses and the upper/lower bounds used for fitting the absorption of the four R6G films are listed in Table 1 (see Appendix).

From Fig. 3 one can clearly see that the spectral shape of film absorption changed significantly with increasing target concentration of R6G. For the lowest concentration (0.2 mol/L), the main peak (~ 540 nm) is showing higher absorption compared to the vibronic shoulder (~ 503 nm) as can be seen in Fig. 3(a). However, with increasing concentration, the vibronic shoulder gets more and more dominant in absorption and becoming a peak of its own as one can see in Figs. 3(b) and 3(c). The linewidths also broaden for both peaks (~ 540 nm and ~ 503 nm) with increasing concentration. Finally, for the highest concentration (5.2 mol/L), the absorption spectrum evolves into a flat top profile as shown in Fig. 3(d). That is because the rise in the absorption of the main peak is relatively less significant compared to that of the vibronic shoulder when concentration is increased. The broadening of both peaks further accelerates the merging of two separate peaks into a flat and wide spectral profile. Absorbance of dye molecules is linearly proportional with the molecular concentration and at high concentration, different intermolecular interactions (not limited to aggregation) can have different contributions leading to an inhomogeneous broadening of the absorption profile. Therefore, our observed changes (hike in absorbance and broadening) in the absorption due to the increase in concentration are consistent with the known effects of molecular systems reported earlier [14,24].

Considering the fact that spectral evolution of the two peaks is different when concentration is varied, we employed LOM and MLOM fitting (with identical initial guesses and physical constraints) on the experimental absorption spectra. It is evident from the figure that for all concentrations, $A_{TMM(MLOM)}$ outperforms $A_{TMM(LOM)}$ by providing a better agreement with A_{exp}. Such finding clearly indicates that an increase in the molecular concentration results in the excitonic absorption bands, which are neither a true Lorentzian nor a pure Gaussian [19], and therefore, utilizing the frequency-dependent inhomogeneous broadening function is the only way to fit such absorption profiles as shown by our MLOM fitting. A quantitative picture of our finding is depicted in Fig. 4 where the values of Θ for each cases are reported (in $\log_{10}$ scale for better visualization) as a function of R6G concentration. It further confirms the superiority of MLOM over LOM in terms of minimal Θ. However, in both LOM and MLOM, the value of Θ is increasing with increasing concentration, indicating the challenge of maintaining accuracy of the methods for extremely high concentrated molecular films.

The effect of R6G concentration on the optimal fitting parameters of MLOM can be inferred from Fig. 5 with the optimal values reported in Table 1 (see Appendix). The optimal oscillator strengths (f_j) as a function of R6G concentration are depicted (in $\log_{10}$ scale for better visualization) in Fig. 5(a). From the figure, we can see that the oscillator strength of the vibronic shoulder (f_2) is lower than that of the molecular resonance (f_1) for the lowest concentration. An increase in R6G concentration causes a significant rise in f_2 leading to a scenario where $f_2 > f_1$ manifested as a rise of the vibronic shoulder in the corresponding absorption profiles. In Fig. 5(b), one can see that with increasing concentration, the peak positions (E_j) of both the molecular resonance (E_1) and its vibronic shoulder (E_2) are shifting towards lower energy implying a spectral red shift in the wavelength scale. The separation between the peaks is also increasing with the concentration. At high concentration of dye molecules, the absorption bands experience spectral red shift due to various intermolecular dipolar interactions (e.g. formation of aggregates) leading to a reduction in the effective oscillation frequency of the molecular system (i.e. red shift in wavelength scale). The increasing separation between the main and shoulder peaks due to rise in concentration can be addressed with the help of quantum mechanics considering interactions between dye molecules as repulsive energy eigenstates in a perturbative scenario. Hence, all the observed trends are known spectroscopic features of dye molecules [14,24].

Optical Materials EXPRESS

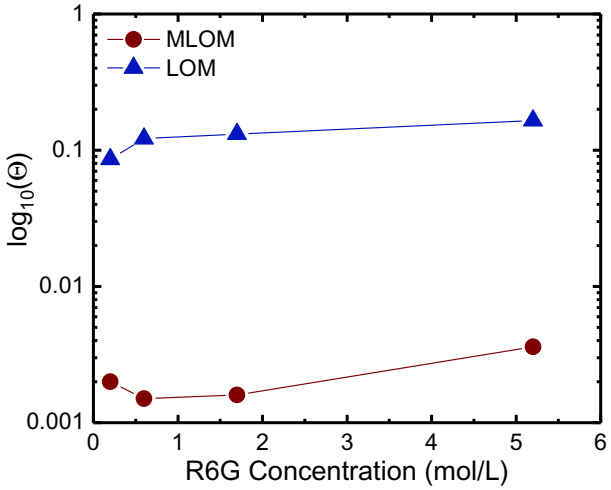

Fig. 4. Evolution of Θ (in $\log_{10}$ scale) as a function of R6G concentration. The blue triangles and red circles connected by lines of corresponding color depict the discrete data points.

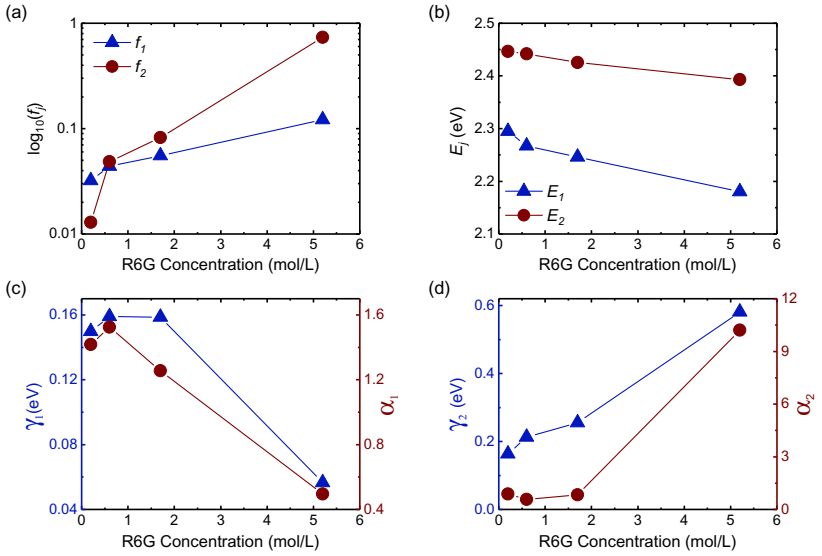

Fig. 5. Evolution of (a) f_j (in $\log_{10}$ scale), (b) E_j, (c) γ_1 and α_1, and (d) γ_2 and α_2 as a function of R6G concentration. In the figure, $j = 1$ and $j = 2$ represent the molecular resonance (~ 540 nm) and the vibronic shoulder (~ 503 nm) of R6G, respectively. The blue triangles and red circles connected by lines of corresponding color depict the discrete data points. In (c)-(d), the blue and red vertical axes correspond to the blue and red data points, respectively.

Optical Materials EXPRESS

An insight on the role of the adjustable broadening function (γ_j') can be developed from Figs. 5(c) and 5(d) where Fig. 5(c) depicts the evolution of the broadening parameters (γ_j and α_j) as a function of R6G concentration for the molecular resonance (γ_1 and α_1), while Fig. 5(d) shows the same for the vibronic shoulder (γ_2 and α_2). From Fig. 5(c) it is clear that both γ_1 and α_1 are initially increased as the concentration increases from 0.2 mol/L to 0.6 mol/L, but both drop unintuitively for the high concentrations (1.7 mol/L and 5.2 mol/L). On the other hand, Fig. 5(d) shows that the broadening parameters of the vibronic shoulder (γ_2 and α_2) are increasing with respect to the concentration validating its dominance at high concentrations. The aforementioned trend could, however, be exaggerated by the fitting, but it is also challenging to interpret spectroscopically since it requires further studies on the molecular aggregates formed at high concentrations, which is outside the scope of this article.

The optimal α_j values for both the molecular resonance (α_1) and the vibronic shoulder (α_2) are higher than 0.4 for all R6G films (see Table 1 in Appendix) indicating that the spectral nature of γ_j' is neither a true Lorentzian ($\alpha_j = 0$) nor a pure Gaussian ($\alpha_j \approx 0.3$) but an asymmetric lineshape instead [19].

It is worth to mention here that our MLOM approach is preferable not only over the use of convolution of different spectral functions (Gaussian/Voigt) which lacks analytically closed form but also over the use of higher number of oscillators in the conventional LOM since earlier studies have shown that the fit quality does not improve significantly with the increased number of oscillators compared to the use of a frequency-dependent adjustable broadening function [19,25].

The optical constants of the R6G films evaluated from the optimal MLOM show a similar trend to the one found for R6G molecules in solutions [43] and in dry solid film [44,45]. The dispersion of the complex dielectric function (ϵ) and the complex refractive index (N) for the four R6G films are reported in Fig. 6 and Fig. 7, respectively, while Fig. 8 reports the experimental optical constants of a R6G film reproduced from existing literature [45] for a better visual comparison.

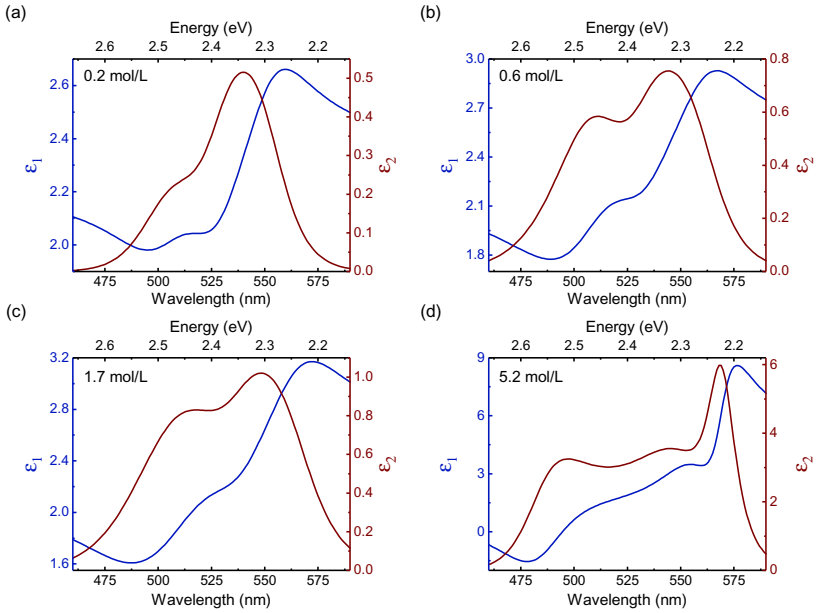

Fig. 6. Real (ϵ_1) and imaginary (ϵ_2) parts of the complex dielectric function (ϵ) of the R6G films in the spectral range of the local excitonic band of interest for target concentrations: (a) 0.2 mol/L, (b) 0.6 mol/L, (c) 1.7 mol/L and (d) 5.2 mol/L. The blue and red vertical axes correspond to the blue and red curves, respectively.

Optical Materials EXPRESS

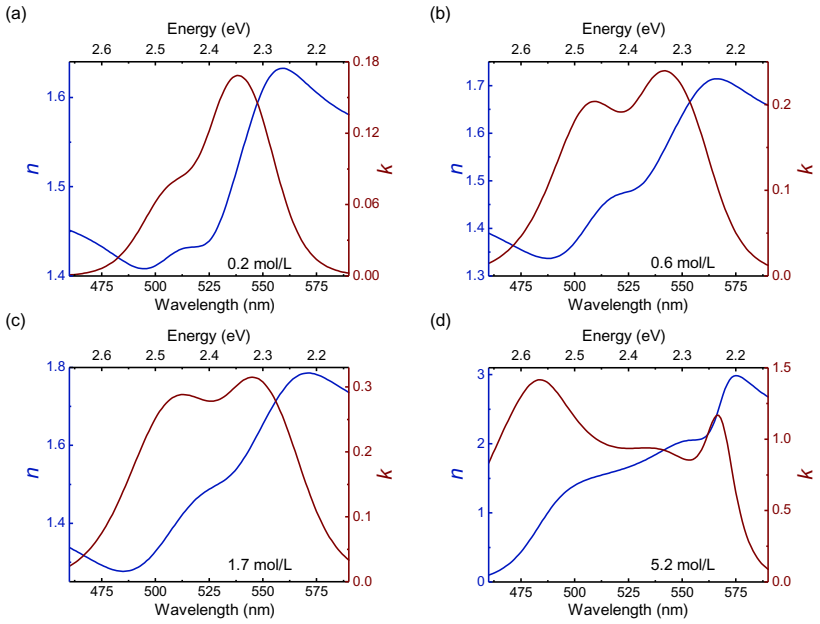

Fig. 7. Real (n) and imaginary (k) parts of the complex refractive index (N) of the R6G films in the spectral range of the local excitonic band of interest for target concentrations: (a) 0.2 mol/L, (b) 0.6 mol/L, (c) 1.7 mol/L and (d) 5.2 mol/L. The blue and red vertical axes correspond to the blue and red curves, respectively.

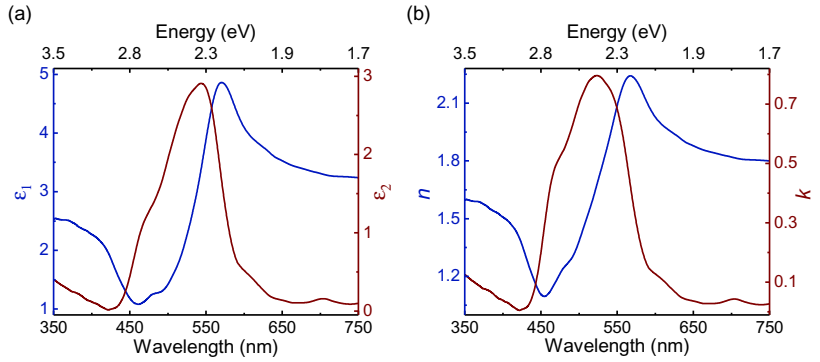

Fig. 8. Experimental complex (a) dielectric function ($\epsilon = \epsilon_1 + i\epsilon_2$) and (b) refractive index ($N = n + ik$) of R6G reproduced from Ref. [45]. The blue and red vertical axes correspond to the blue and red curves, respectively.

Optical Materials EXPRESS

From Figs. 6 and 7 we can clearly see that the imaginary parts of ϵ and N, i.e., ϵ_2 and k, closely follow the absorption profiles of the films - except in the highest concentration where they show interesting profile with three peaks, which reveals that the exciton landscape is changing within these concentrations. However, in all samples the values of ϵ_2 and k are monotonically increasing with increasing concentration, in accordance with the absorption. The real parts of ϵ and N, i.e., ϵ_1 and n, show a similar trend in their values with respect to the concentration. In addition, the difference between the magnitudes of n in the blue and red regions of the spectrum is increasing with concentration. Similar nature is found in ϵ_1 which becomes negative, implying metallic like behavior [8,44], in the 460 nm - 500 nm region for the highest concentration sample as shown in Fig. 6(d). The dispersion of both the real and the imaginary components of N and ϵ, over the spectral region of interest, for all concentrations, show a similar qualitative nature to the one reported in the existing literature [45] as shown in Fig. 8 and to the one found in dye-doped excitonic films in general [8,25,44,46].

It is worth of noting that the exact values of the optical constants we report here for R6G cannot be generalized for arbitrary R6G doped films since depending on the molecular concentration, film thickness, type of the hosting polymer and any anisotropy in the film quality, the film absorption and consequently, the extracted optical constants can drastically differ from our case. Nevertheless, we have successfully demonstrated here a straightforward way to determine the optical constants of dye doped isotropic excitonic thin films directly from their absorption spectra without ellipsometry. Our method outperforms the conventional LOM in terms of fitting accuracy and can be easily generalized to many other isotropic excitonic thin films. Our findings are important in the context of designing photonic and optoelectronic devices based on organic materials where modeling of local excitonic absorption bands of organic thin films is crucial.

5. Conclusions

In this work, we reported a method to evaluate the complex-dispersive retractive index and dielectric function of isotropic organic thin films from their absorption spectra without ellipsometry. We used a spectral fitting approach which contains a MLOM and an optimization algorithm to minimize an objective function representing the degree of dissimilarity between the experimental and the fitted curve. The MLOM differs from the conventional LOM by employing a frequency-dependent adjustable broadening function in the damping rate term and hence, can fit any inhomogeneous spectral broadening other than Lorentzian, Gaussian or Voigt profiles. Our method was implemented via TMM to extract the optical constants of R6G:PVA films with varying R6G concentration.

Our findings quantitatively showed that MLOM can outperform LOM in terms of fitting accuracy, especially when the molecular concentration is very high. The effect of concentration on the MLOM parameters was also analyzed, and it validated the corresponding spectral changes in the experimental absorption. Our evaluated optical constants and their dispersion are in good agreement with the qualitative trend found in other excitonic thin films. Our findings provide a way to determine the optical constants of organic thin films and hence, to model their local excitonic absorption bands which is crucial in designing excitonic and polaritonic devices for organic nanophotonics.

Optical Materials EXPRESS

Appendix

Table 1. Initial guesses and physical constraints of the fitting parameters, as well as the final fitted values, in MLOM and LOM (except α_j) for R6G films with different concentrations. Two-oscillator model was employed in the fitting to implement the R6G absorption having a molecular resonance at E_1 = 2.30 eV (540 nm) and a vibronic shoulder at E_2 = 2.46 eV (503 nm). Other parameters related to corresponding resonant energy E_j, are oscillator strength f_j, damping rate γ_j and adjustable broadening parameter α_j.

Conc. (mol/L)	Parameters	Initial guess	Lower bound	Upper bound	Fitted value
0.20	f_1	0.05	0.01	0.10	0.0320
	f_2	0.05	0.01	0.10	0.0129
	γ_1 (eV)	0.30	0.10	0.50	0.1497
	γ_2 (eV)	0.30	0.10	0.50	0.1633
	E_1 (eV)	2.30	2.25	2.35	2.2946
	E_2 (eV)	2.45	2.40	2.50	2.4468
	α_1	2.50	0.01	5.00	1.4171
	α_2	2.50	0.01	5.00	0.8727
0.60	f_1	0.05	0.01	0.10	0.0439
	f_2	0.05	0.01	0.10	0.0486
	γ_1 (eV)	0.30	0.10	0.50	0.1590
	γ_2 (eV)	0.30	0.10	0.50	0.2129
	E_1 (eV)	2.26	2.24	2.28	2.2670
	E_2 (eV)	2.45	2.40	2.50	2.4419
	α_1	2.50	0.01	5.00	1.5246
	α_2	2.50	0.01	5.00	0.5771
1.70	f_1	0.05	0.01	0.10	0.0554
	f_2	0.05	0.01	0.10	0.0824
	γ_1 (eV)	0.30	0.10	0.50	0.1586
	γ_2 (eV)	0.30	0.10	0.50	0.2548
	E_1 (eV)	2.24	2.20	2.28	2.2459
	E_2 (eV)	2.45	2.40	2.50	2.4252
	α_1	2.50	0.01	5.00	1.2550
	α_2	2.50	0.01	5.00	0.8362
5.20	f_1	0.25	0.01	1.00	0.1216
	f_2	0.25	0.01	1.00	0.7330
	γ_1 (eV)	0.25	0.01	1.00	0.0565
	γ_2 (eV)	0.25	0.01	1.00	0.5807
	E_1 (eV)	2.20	2.00	2.40	2.1802
	E_2 (eV)	2.46	2.26	2.66	2.3931
	α_1	7.50	0.01	15.00	0.4954
	α_2	7.50	0.01	15.00	10.2070

Optical Materials EXPRESS

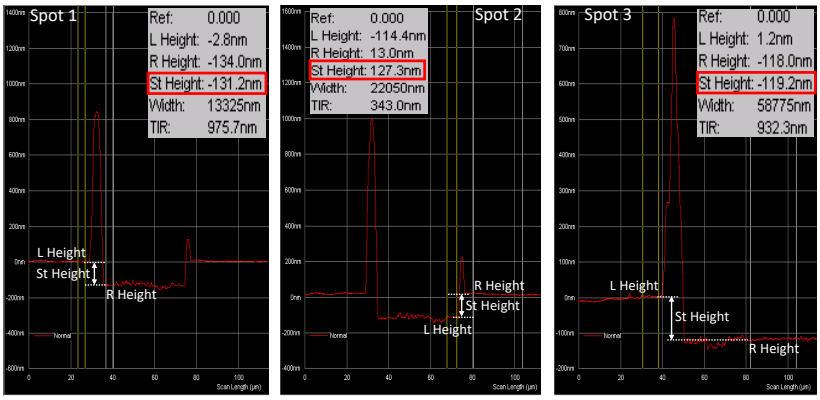

Fig. 9. Profilometer data for R6G:PVA film with target concentration 0.2 mol/L. The film thickness was measured by creating a score on the film and was estimated as the height difference (St height) between the right (R height) and left (L height) sides of the score edge. Thickness was measured at three different spots (131.2 nm, 127.3 nm, and 119.2 nm) along the score edge and the average value (125.9 nm, i.e., ~ 125 nm) was considered in TMM calculation.

Funding. Academy of Finland (289947, 323995).

Acknowledgments. The authors thank Dr. Henry A. Fernandez (Department of Electronics and Nanoengineering, Aalto University, Finland) for his helpful suggestions during the research work.

Disclosures. The authors declare no conflicts of interest.

Data availability. Data underlying the results presented in this paper are not publicly available at this time but may be obtained from the authors upon reasonable request.

References

1. O. Inganäs, "Organic photovoltaics over three decades," Adv. Mater. **30**(35), 1800388 (2018).
2. Z. Li, X. Zhao, X. Lu, Z. Gao, B. Mi, and W. Huang, "Organic thin-film solar cells: devices and materials," Sci. China Chem. **55**(4), 553–578 (2012).
3. Y. Cui, H. Yao, L. Hong, T. Zhang, Y. Tang, B. Lin, K. Xian, B. Gao, C. An, P. Bi, W. Ma, and J. Hou, "Organic photovoltaic cell with 17% efficiency and superior processability," Natl. Sci. Rev. **7**(7), 1239–1246 (2020).
4. O. Ostroverkhova, "Organic optoelectronic materials: mechanisms and applications," Chem. Rev. **116**(22), 13279–13412 (2016).
5. I. D. W. Samuel and G. A. Turnbull, "Organic semiconductor lasers," Chem. Rev. **107**(4), 1272–1295 (2007).
6. S. Tanida, K. Noda, H. Kawabata, and K. Matsushige, "N-channel thin-film transistors based on 1, 4, 5, 8-naphthalene tetracarboxylic dianhydride with ultrathin polymer gate buffer layer," Thin Solid Films **518**(2), 571–574 (2009).
7. S. K. Saikin, A. Eisfeld, S. Valleau, and A. Aspuru-Guzik, "Photonics meets excitonics: natural and artificial molecular aggregates," Nanophotonics **2**(1), 21–38 (2013).
8. M. J. Gentile, S. Nú nez-Sánchez, and W. L. Barnes, "Optical field-enhancement and subwavelength field-confinement using excitonic nanostructures," Nano Lett. **14**(5), 2339–2344 (2014).
9. M. J. Gentile, S. A. R. Horsley, and W. L. Barnes, "Localized exciton-polariton modes in dye-doped nanospheres: a quantum approach," J. Opt. **18**(1), 015001 (2016).
10. A. Canales, D. G. Baranov, T. J. Antosiewicz, and T. Shegai, "Abundance of cavity-free polaritonic states in resonant materials and nanostructures," J. Chem. Phys. **154**(2), 024701 (2021).
11. C. J. Bardeen, "The structure and dynamics of molecular excitons," Annu. Rev. Phys. Chem. **65**(1), 127–148 (2014).
12. M. Nyman, A. Shevchenko, I. Shavrin, Y. Ando, K. Lindfors, and M. Kaivola, "Large-area enhancement of far-field fluorescence intensity using planar nanostructures," APL Photonics **4**(7), 076101 (2019).
13. A. Dutta, V. Tiainen, and J. J. Toppari, "Optimizing geometry of low-Q all-metal Fabry-Pérot microcavity for fluorescence spectroscopy," IOP SciNotes **2**(1), 015205 (2021).
14. S. V. Baieva, T. K. Hakala, and J. J. Toppari, "Strong coupling between surface plasmon polaritons and sulforhodamine 101 dye," Nanoscale Res. Lett. **7**(1), 191 (2012).
15. P. A. Hobson, W. L. Barnes, D. G. Lidzey, G. A. Gehring, D. M. Whittaker, M. S. Skolnick, and S. Walker, "Strong exciton-photon coupling in a low-Q all-metal mirror microcavity," Appl. Phys. Lett. **81**(19), 3519–3521 (2002).
16. E. Hulkko, S. Pikker, V. Tiainen, R. H. Tichauer, G. Groenhof, and J. J. Toppari, "Effect of molecular stokes shift on polariton dynamics," J. Chem. Phys. **154**(15), 154303 (2021).

Optical Materials EXPRESS

17. D. S. Dovzhenko, S. V. Ryabchuk, Y. P. Rakovich, and I. R. Nabiev, "Light-matter interaction in the strong coupling regime: configurations, conditions, and applications," Nanoscale **10**(8), 3589–3605 (2018).
18. D. Poelman and P. F. Smet, "Methods for the determination of the optical constants of thin films from single transmission measurements: a critical review," J. Phys. D: Appl. Phys. **36**(15), 1850–1857 (2003).
19. A. B. Djurišić, T. Fritz, and K. Leo, "Modelling the optical constants of organic thin films: impact of the choice of objective function," J. Opt. A: Pure Appl. Opt. **2**(5), 458–464 (2000).
20. S. S. Falahatgar and F. E. Ghodsi, "A developed model for the determination of the dielectric function for some absorbing thin films using pseudo-Urbach tail," Phys. B **412**, 4–11 (2013).
21. I. Chambouleyron and J. M. Martínez, "Optical properties of dielectric and semiconductor thin films, in *Handbook of Thin Films: Volume 3*, H. S. Nalwa, ed. (Academic Press, 2002).
22. H. Fujiwara, *Spectroscopic Ellipsometry: Principles and Applications* (Wiley, 2007).
23. H. G. Tompkins and J. N. Hilfiker, *Spectroscopic Ellipsometry: Practical Application to Thin Film Characterization* (Momentum Press, 2015).
24. C. On, E. K. Tanyi, E. Harrison, and M. A. Noginov, "Effect of molecular concentration on spectroscopic properties of poly(methyl methacrylate) thin films doped with rhodamine 6G dye," Opt. Mater. Express **7**(12), 4286–4295 (2017).
25. A. B. Djurišić, T. Fritz, and K. Leo, "Modeling the optical constants of organic thin films: application to 3, 4, 9, 10-perylenetetracarboxylic dianhydride (PTCDA)," Opt. Commun. **183**(1-4), 123–132 (2000).
26. C. C. Kim, J. W. Garland, H. Abad, and P. M. Raccah, "Modeling the optical dielectric function of semiconductors: extension of the critical-point parabolic-band approximation," Phys. Rev. B **45**(20), 11749–11767 (1992).
27. A. Franke, A. Stendal, O. Stenzel, and C. von Borczyskowski, "Gaussian quadrature approach to the calculation of the optical constants in the vicinity of inhomogeneously broadened absorption lines," Pure Appl. Opt. **5**(6), 845–853 (1996).
28. M. V. Bondar, O. V. Przhonska, and Y. A. Tikhonov, "Inhomogeneous broadening of organic dyes in polymeric media: nonlinear transmission spectra and photochemical kinetics," J. Phys. Chem. **96**(26), 10831–10837 (1992).
29. S. T. Hoffmann, H. Bässler, and A. Köhler, "What determines inhomogeneous broadening of electronic transitions in conjugated polymers?" J. Phys. Chem. B **114**(51), 17037–17048 (2010).
30. D. Gonçalves and E. A. Irene, "Fundamentals and applications of spectroscopic ellipsometry," Quím. Nova **25**(5), 794–800 (2002).
31. G. Jungk, "Possibilities and limitations of ellipsometry," Thin Solid Films **234**(1-2), 428–431 (1993).
32. J. S. Schildkraut, "Limitations to the determination of the optical properties of a thin film by combined ellipsometric and surface plasmon resonance measurements," Appl. Opt. **27**(16), 3329–3333 (1988).
33. P. Markoš and C. M. Soukoulis, *Wave Propagation: From Electrons to Photonic Crystals and Left-Handed Materials* (Princeton University Press, 2008).
34. T. G. Mackay and A. Lakhtakia, *The Transfer-Matrix Method in Electromagnetics and Optics* (Morgan and Claypool, 2020).
35. R. B. Balili, "Transfer matrix method in nanophotonics," Int. J. Mod. Phys. Conf. Ser. **17**, 159–168 (2012).
36. K. J. Pascoe, "Reflectivity and transmissivity through layered, lossy media: a user-friendly approach," Tech. rep., Air Force Institute of Technology, Wright-Patterson Air Force Base (2001).
37. https://www.mathworks.com/products/matlab.html.
38. H. Sumi and Y. Kayanuma, "Is the Lorentz model applicable to optical absorption by excitons?" Solid State Commun. **85**(1), 1–4 (1993).
39. https://www.mathworks.com/help/optim/ug/fmincon.html.
40. S. M. Abrarov and B. M. Quine, "A rational approximation for efficient computation of the Voigt function in quantitative spectroscopy," J. Math. Res. **7**(2), 163–174 (2015).
41. B. L. Darby, B. Auguié, M. Meyer, A. E. Pantoja, and E. C. Le Ru, "Modified optical absorption of molecules on metallic nanoparticles at sub-monolayer coverage," Nat. Photonics **10**(1), 40–45 (2016).
42. M. J. Schnepf, M. Mayer, C. Kuttner, M. Tebbe, D. Wolf, M. Dulle, T. Altantzis, P. Formanek, S. Förster, S. Bals, T. A. F. König, and A. Fery, "Nanorattles with tailored electric field enhancement," Nanoscale **9**(27), 9376–9385 (2017).
43. W. Leupacher and A. Penzkofer, "Refractive-index measurement of absorbing condensed media," Appl. Opt. **23**(10), 1554–1558 (1984).
44. L. Gu, J. Livenere, G. Zhu, E. E. Narimanov, and M. A. Noginov, "Quest for organic plasmonics," Appl. Phys. Lett. **103**(2), 021104 (2013).
45. T. Itoh, Y. S. Yamamoto, and T. Okamoto, "Anti-crossing property of strong coupling system of silver nanoparticle dimers coated with thin dye molecular films analyzed by electromagnetism," J. Chem. Phys. **152**(5), 054710 (2020).
46. E. G. Bortchagovsky and U. C. Fischer, "Method for determination of the dielectric function of a thin absorbing film on variable substrates from transmission spectra," Appl. Opt. **42**(34), 6915–6918 (2003).